The Albedo, Effective Temperature, and Energy Balance of Uranus, as Determined from Voyager IRIS Data

J. C. PEARL, B. J. CONRATH, R. A. HANEL, AND J. A. PIRRAGLIA

NASA/Goddard Space Flight Center, Greenbelt, Maryland 20771

AND

A. COUSTENIS

Observatoire de Paris, Meudon, France

Data from the Voyager infrared spectrometer and radiometer (IRIS) investigation are used to determine the albedo, effective temperature, and energy balance of Uranus. From broadband radiometric observations made over a range of phase angles $15° < \alpha < 155°$, an orbital mean value for the bolometric Bond albedo, $\overline{A} = 0.300 \pm 0.049$, is obtained, which yields an equilibrium temperature $T_{eq} = 58.2 \pm 1.0°K$. From thermal spectra obtained over latitudes from pole to pole, an effective temperature $T_{eff} = 59.1 \pm 0.3°K$ is derived. This represents a substantial improvement over previously determined values. The energy balance of Uranus is therefore $E = 1.06 \pm 0.08$; the one-standard-error upper limit of 1.14 is lower than previous results. © 1990 Academic Press, Inc.

1. INTRODUCTION

Energy flux from a planetary interior provides significant information on the state of evolution of the planet. The difference between the emitted thermal and the absorbed solar flux, normally expressed as the "energy balance" (the ratio of these quantities), has been determined for all of the major planets, though with differing precision.

Previous ground-based and spacecraft observations have revealed large excess energy fluxes from Jupiter and Saturn. Jupiter emits 1.67 times as much energy in the infrared as it absorbs from the Sun (Hanel *et al.* 1981). This excess is primarily due to primordial heat liberated during the quasiadiabatic collapse phase of Jovian formation (Graboske *et al.* 1975) and in part due to gravitational energy released during the precipitation of helium in the metallic

hydrogen core (Smoluchowski 1967, Salpeter 1973, Hubbard and Smoluchowski 1973, Stevenson and Salpeter 1976, Pollack *et al.* 1977). For Saturn the ratio of emitted to absorbed energy is 1.78 (Hanel *et al.* 1983). Evolutionary models suggest that Saturn, smaller and less massive than Jupiter, has lost most of its primordial heat, leaving helium separation as the dominant heat generating mechanism. This conclusion is supported by the low helium abundance in the observable layers of Saturn's atmosphere (mass fraction 0.06 ± 0.05; Conrath *et al.* 1984) relative to that found on Uranus (0.26 ± 0.08; Hanel *et al.* 1986, Conrath *et al.* 1987). Jupiter (0.18 ± 0.04; Gautier *et al.* 1981) is intermediate between Saturn and Uranus.

Estimates of the Uranian energy balance to date permit only a relatively weak internal heat source. By using recent spectro-

TABLE I

DETERMINATIONS OF THE ALBEDO AND ENERGY BALANCE OF URANUS

Reference	p	q	A	T_{eff}	Energy balance
Lockwood *et al* (1983)	0.262 ± 0.008^{a}	$1\ 50^{+0\ 14}_{-0\ 17}$	$0.348 - 0\ 430$	$57\ 0 \pm 2\ 5^{b}$	$<1\ 24$
Neff *et al.* (1985)	$0.28\ \pm 0\ 02^{a}$	$1\ 2$	$0\ 34\ \pm 0\ 02$	$58.6 \pm 2\ 0^{c}$	$<1\ 48$
Pollack *et al* (1986)^{d}	$0\ 253 \pm 0.046$	$1\ 26 \pm 0.11$	0.319 ± 0.051	$57.7 \pm 2\ 0^{e}$	$<1\ 27$
This investigation^{d}	$0.215 \pm 0\ 046$	1.40 ± 0.14	$0\ 300 \pm 0.049$	59.1 ± 0.3	$<1\ 14$

^{a} For epoch 1981
^{b} Courtin *et al* (1979)
^{c} Hildebrand *et al* (1985)
^{d} Using annual mean values for p and A.
^{e} Orton (1985)

photometric observations, Lockwood *et al.* (1983) derive a geometric albedo of 0.262 ± 0.008 for the epoch 1981; assuming that the phase integral is between 1.33 and 1.64 yields a Bond albedo between 0.348 and 0.430. By combining this with the effective temperature of 57.0 ± 2.5°K determined by Courtin *et al.* (1979), Lockwood *et al.* obtain an upper limit of 1.24 for the Uranian energy balance. The principal uncertainties are in the phase function and the thermal emission (Table I). Neff *et al.* (1985), using visible and near-infrared spectrophotometry, obtain a geometric albedo of 0.28 ± 0.02 for the same epoch. Assuming a phase integral of 1.2 and using the effective temperature of 58.6 ± 2°K from Hildebrand *et al.* (1985), Neff *et al.* find a value of the Uranian heat source of (0.6 ± 1.4) × 10^{15} W, which corresponds to an energy balance of 1.11 ± 0.37 or an upper limit of 1.48. Pollack *et al.* (1986) using the data of Neff *et al.* (1985) and extensive model calculations find a phase integral of 1.26 ± 0.11, which leads to a Bond albedo of 0.319 ± 0.051. With an effective temperature of 57.7 ± 2°K (Orton 1985) the upper limit for the energy balance is 1.27. The main conclusions of these recent determinations are summarized in Table I.

The data for the present investigation were obtained by the Infrared Interferometer Spectrometer (IRIS) between January 15 and February 2, 1986, during the Voyager 2 flyby of Uranus. We estimate the bolometric Bond albedo for this epoch from measurements of the reflected radiation observed by the IRIS radiometer. The thermal emission of the planet is estimated from spectra obtained by the infrared interferometer, extrapolated by the use of models to spectral regions not covered by the instrument. After making adjustments for seasonal effects, the energy balance and intrinsic luminosity of Uranus are determined from the emitted thermal and absorbed solar energies. In Section 2 pertinent details of the instrumentation are discussed. In Section 3 we determine the Bond albedo. The thermal emission is derived in Section 4. The energy balance is derived, and the results are discussed in Section 5.

2. INSTRUMENTATION AND CALIBRATION

The IRIS on both Voyager spacecraft are described by Hanel *et al.* (1980). Incoming radiation is collected by the 50-cm diameter primary mirror of a Cassegrain telescope and directed through a field-limiting aperture to define a 0.25° diameter beam. The infrared portion of this beam is reflected by a dichroic mirror toward the interferometer, while the visible radiation is transmitted to the single-channel radiometer.

The interferometer provides thermal spectra over a useful spectral range from 180 cm^{-1} to an upper limit determined by the very low temperatures of the outer

TABLE II

OBSERVATIONS OF THE TARGET PLATE USED FOR IRIS RADIOMETER CALIBRATION

Observation	Date	Sun–spacecraft range (AU)	Signal, viewing target plate (DN)[a]	Distance scaled signal (DN × AU²)
Before Jupiter	15 April, 1979	4 969 73	1 263 ± 1 4	31 194 ± 49
After Jupiter	26 Oct., 1979	5.751 40	943 ± 1.4	31 193 ± 66
Before Saturn	16 April, 1981	8.748 38	407 ± 1 4	31 149 ± 153
After Saturn[b]	—	—	—	—
Before Uranus	16 Oct., 1985	18.278 85	92 ± 1 4	30 739 ± 668
After Uranus	20 Feb., 1986	19.309 36	85 ± 1 4	31 692 ± 746

[a] The 1.4 DN uncertainty incorporates errors due to quantization, nonlinearity, and baseline drift in the system

[b] No calibration maneuver was performed after the Saturn encounter because of problems manipulating the scan platform.

planets (approximately 400 cm⁻¹ at Uranus). The data are calibrated for each spectral interval at an apodized resolution of 4.3 cm⁻¹ by scaling the planetary radiance to those of deep space and a blackbody function corresponding to the instrument temperature (Hanel et al. 1980, 1981).

The broadband radiometer data (5600–33,000 cm⁻¹) are calibrated by referencing to observations of a spacecraft-mounted diffusely scattering target plate of known reflective properties. For all such measurements, the plate is illuminated by the Sun at 30° to the surface normal. Observations for the Voyager 2 radiometer are listed in Table II. If the radiometer and target plate underwent no temporal changes, then the product of the radiometer signal times the square of the Sun–spacecraft distance, which represents the radiometer signal scaled to 1 AU, would remain constant. The 1-AU radiometer signals calculated from the data are listed in the table, and are plotted in Fig. 1.[1] Within the uncertainties

[1] We plot quantities related to radiometer measurements in terms of instrument data numbers (DN) in order to isolate and display various sources of error By following this procedure, the significant errors in Fig 1 are due only to quantization uncertainties, and in Fig 3 to quantization and pointing uncertainties Systematic errors due to modeling, and uncertainties associated with the transformation from DN to albedo, are then considered separately, as discussed below

in the radiometer measurements, no degradation has occurred over the duration of the mission. This is in contrast to the behavior of the Voyager 1 radiometer system (also plotted in Fig. 1), which showed a possible secular deterioration, together with a significant drop as a result of deep penetration into the intense Jovian radiation environment by that spacecraft (Hanel et al. 1983); the more distant encounter of Jupiter by the second spacecraft (at 10.1 R_J, rather than 4.9 R_J) apparently prevented similar degradation in the combined system of radiometer plus target plate on Voyager 2. We consider it unlikely that precisely compensating changes have occurred in the target plate and in the radiometer; we therefore assume that the properties of both the plate and the radiometer have remained stable throughout the mission.

The distance-scaled radiometer signal is necessary for determination of the radiometer sensitivity, which is required for evaluation of the bolometric Bond albedo (Section 3). To determine its value at Uranus requires defining the calibration in the presence of increasingly large relative quantization uncertainties. The average of all of the measurements in Table II, weighted by the inverse squares of their relative uncertainties (31191 ± 38 DN) gives excessive weight to the early data, as well as an unre-
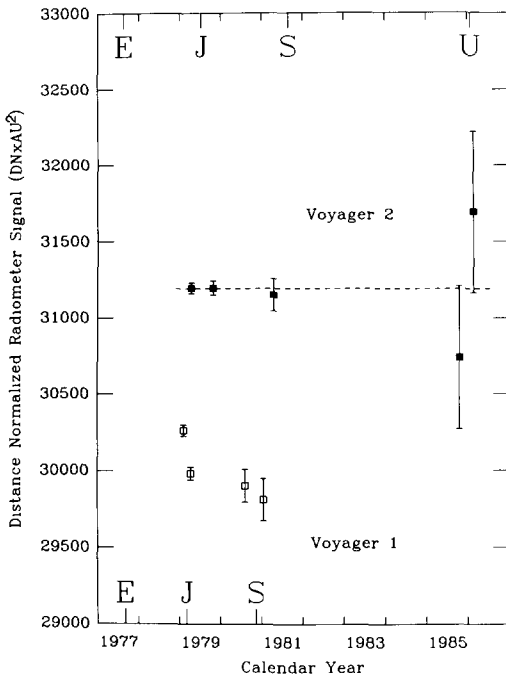
FIG 1 IRIS radiometer signals from target plate observations, normalized to 1 AU (open points: Voyager 1; solid points. Voyager 2), all measurements are made with the target plate normal oriented at 30° to the incident solar flux vector. The error flags represent uncertainties due to quantization, nonlinearity, and baseline drift. As signals drop due to increasing Sun-spacecraft distance, relative errors increase, at Uranus, a toggle of 1 DN in each measurement could bring the data points nearly to the average. (The horizontal dashed line represents the average of all Voyager 2 measurements.) The radiometer system on the Voyager 2 instrument has shown no degradation; that on Voyager 1 was adversely affected by the radiation environment of Jupiter, due to the close flyby of the planet Launch and encounter dates for the two spacecraft are indicated by E, Earth; J, Jupiter; S, Saturn; and U, Uranus.

alistically small error estimate; using only the two measurements near Uranus (31163 ± 498 DN) represents the opposite extreme. We therefore adopt the equally weighted average of all data, with a 1% uncertainty (31193 ± 312 DN) as a realistic estimate of the accuracy and precision of the equivalent 1-AU radiometer signal at Uranus.

3. BOND ALBEDO

In order to determine the Bond albedo of Uranus at the time of the Voyager encounter, we first establish the absolute phase curve. Ideally, this would be obtained through a series of calibrated full-disk measurements over the complete range of phase angles. Voyager IRIS data, however, were available only for phase angles between 15° and 155°. In addition, full-disk observations were not possible because of the close proximity of the spacecraft to the planet. We therefore calculate the disk brightness based on maps, scans, and crescent observations which were obtained at various phase angles. To accomplish this requires a means of describing the photometric behavior over the disk, given incomplete observational coverage. As we lack a detailed microphysical model of the Uranian atmosphere and aerosols, we parameterize the photometric properties of the planet by the Minnaert function,

$$I = I_0 \, \mu_0^k \, \mu^{k-1},$$

where I is the observed flux; I_0 is the flux under normal viewing and illumination; μ_0 and μ are the cosines of the illuminating and viewing angles, respectively; and k is the limb darkening parameter. To estimate the suitability of such an approach, we have first applied our analysis to the detailed data obtained for Saturn by Tomasko et al. (1980). At each phase angle, the data are fit quite well, except very close to the terminator, where the model underestimates the actual brightness; the intrinsic brightness in this region is low, however, so that the contribution to the disk signal is only on the order of 1% at low and intermediate phase angles.

Direct application of the simple Minnaert model to the Uranian data is not possible, since the planet exhibits significant intrinsic latitudinal variation in brightness (Hanel et al. 1986, Smith et al. 1986). In applying the model, we have chosen to assume that, for
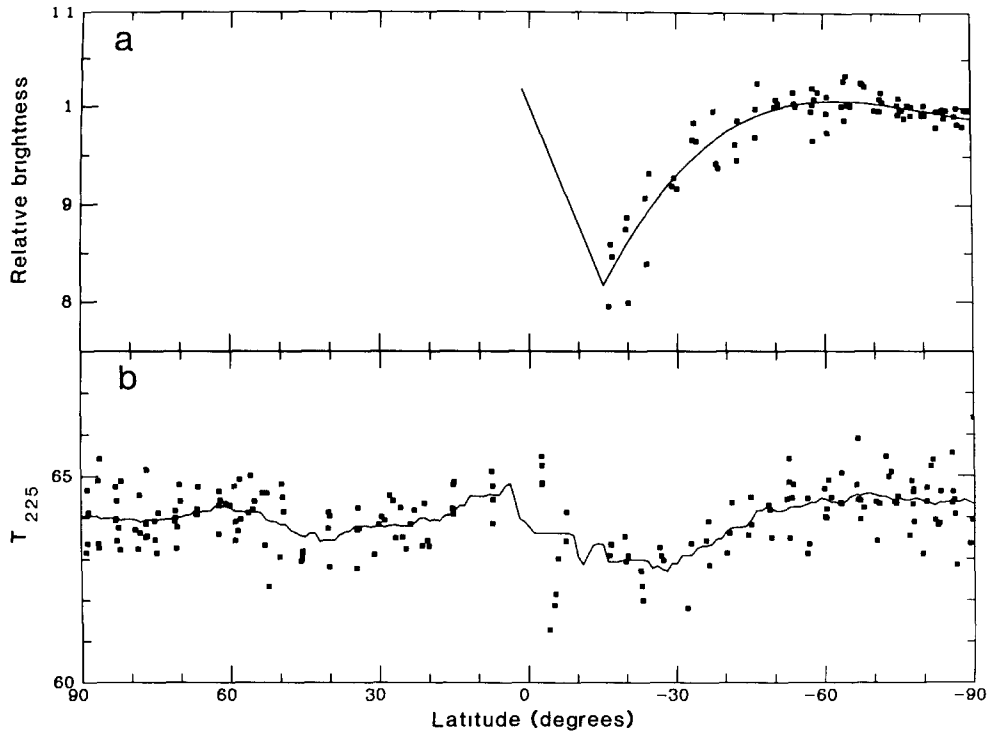
FIG 2 (a) Latitudinal variations in relative reflectivity, normalized to vertical viewing by ratioing
IRIS radiometer data to a Minnaert function fit to data above 45° (see text) For latitudes above 15°, the
curve represents a cubic least-squares fit to the ratio data, for latitudes below 15°, the curve is a linear
representation of the brightening near the terminator seen in images (Smith *et al* 1986) These fits are
used in making evaluations of the disk brightness (b) Latitudinal variations in brightness temperatures
at 225 cm^{-1}, normalized to vertical viewing. (For such geometry, emission at this spectral position
originates in the atmosphere at approximately the radiating level of 400–900 mbar) The curve repre-
sents a running mean over the data in latitude bins 15° wide

the broadband IRIS radiometer data, the
limb darkening parameter is constant over
all latitudes at a given phase angle; devia-
tions from Minnaert behavior are then in-
terpreted as latitudinal variations in the lo-
cal reflectivity.

To establish these variations, we use a
scan at phase angle 21.4°. This scan had
moderate spatial resolution (FOV diameter
0.075 of disk diameter) and progressed dia-
metrically across the disk, normal to the
terminator. In addition, the Voyager Pro-
ject provided refined pointing information,
which had been adjusted to agree precisely
with the pointing deduced from three im-
ages taken during the observation. The

Minnaert model was fit directly only to
those IRIS data with latitudes greater than
45°, since pronounced darkening occurs
equatorward of this. The ratio of each da-
tum to the resulting model calculation is
shown as relative brightness in Fig. 2a. The
superimposed curve, above 15° latitude,
represents a cubic least-squares fit to the
brightness variation. The linear extension
below 15° latitude was chosen to represent
the relative brightening near the terminator,
which is suggested by the Minnaert fits to
limb functions from images (Smith *et al.*
1986); though somewhat crude, the contri-
butions to brightness from very close to the
terminator, where the error is greatest, are

small. This composite fit was used in evaluating the disk signals from all of the maps and scans discussed below. The model disk brightnesses for this and the other observations are listed in Table III, and are plotted in Fig. 3.

Prior to the above measurement, maps and scans were obtained at considerably lower spatial resolution (0.27 to 0.12 of the disk diameter); with corrections for the finite size of the field of view using the Minnaert model, these data were treated as above to provide the disk brightness at their corresponding phase angles (15.3° to 18.3°).

Data at phase angles near 31°, 54°, and 108° consisted of series of observations at fixed latitudes between 15° and 25° south. As above, the derived limb darkening parameter was assumed valid for the entire disk, and the latitudinal albedo variation shown in Fig. 2a was incorporated in evaluating the disk brightness.

As the spacecraft receded from the planet, the phase angle decreased from 155° to its asymptotic value of 145°, many observational sequences were targeted near the center of the crescent. During these observations the width of the crescent center decreased from 0.8 to 0.3 of the diameter of the IRIS field of view; due to pointing drift, the field wandered slowly back and forth across the crescent during these periods. Data were selected for analysis from 20 sets of observations. The maximum signal from each was displayed as a function of phase angle. The upper bounds of this dataset define a smooth envelope; the seven points which fall on or very near this curve are assumed to represent cases where the field of view was positioned to obtain the maximum possible signal (available pointing information is inadequate to determine this independently).

To interpret the radiometer data so selected, the following method was used. Assuming that the brightness distribution in the crescent obeys a Minnaert law with limb darkening parameter k, the expected IRIS radiometer signal was calculated by numerical integration as a function of the position of the field of view relative to the center of Uranus; this was normalized using the signal calculated for the entire crescent. Multiplication of the result by the square of the ratio of the radii of the planet and the projected field of view then repre-

TABLE III

CALCULATED DISK SIGNALS AT LOW AND INTERMEDIATE PHASE
ANGLES, AS DERIVED FROM IRIS RADIOMETER MEASUREMENTS

| Phase angle α (°)	Derived signal (DN)	Limb darkening parameter, k	Remarks
15.8	38.8 ± 2.1	0 85–1 14	Average of 14 scans taken over $15\ 3 \leq \alpha \leq 16\ 8°$
17.8	41 8 ± 2.5	0.82–1 16	Average of 10 scans taken over $17.5 \leq \alpha \leq 18\ 3°$
21.4	41 1 ± 1.5	0.80	Given double weight, since best determined
31 4	32.1 ± 1.9	0.63	Assigned 6% error, based on results of first two averages
54.0	25 1 ± 1 5	0.69	Assigned 6% error, based on results of first two averages
108 0	8 8 ± 0.9	0.78	Error estimate increased to 10%, due to large phase angle change (10°) during observation
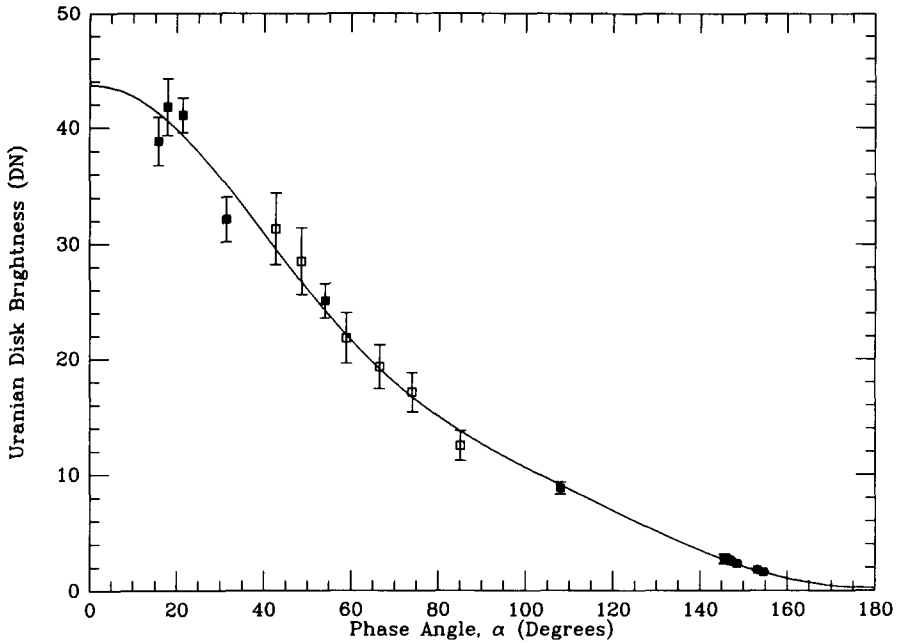
FIG. 3 The phase curve of Uranus in IRIS data numbers (DN) Filled points are derived from IRIS radiometer data, error bars represent only random uncertainties. Open points and their error flags are from imaging data (Pollack *et al.* 1986), normalized by linear interpolation to the IRIS data point at 54° phase angle. The two datasets are quite consistent The solid curve is an interpolant derived by fitting the IRIS data alone (see text)

sents the ratio of the signal from part of the crescent to that of the complete disk. The actual disk signal can then be estimated from an IRIS measurement by use of the scaling relation,

$$I(k, \alpha) = I(\alpha)_{obs} \cdot \left(\frac{r}{R}\right)^2 \cdot \frac{1}{F(k, \alpha)},$$

where $I(k, \alpha)$ is the disk signal at phase angle α, $I(\alpha)_{obs}$ is the observed radiometer signal, r is the projected radius of the field of view, R is the radius of Uranus, and $F(k, \alpha)$ is the model ratio calculated above; for consistency with our data selection criteria, the maximum value of F was used for each evaluation of the disk signal.

The low spatial resolution and inadequate pointing information prevent direct determination of the Minnaert limb darkening parameter, k. However, if it is assumed that k is constant over the relatively small range of phase angles considered here, a value of 0.38 fits the suite of observations; i.e., within a scaling factor, it defines the envelope of the data maxima. Results of our disk brightness calculations, using $k = 0.38$, are listed in Table IV and are plotted in Fig. 3.

The uncertainties listed in Tables III and IV, and shown in Fig. 3, represent our best estimates of random errors. At low phase angles, these are principally associated with pointing and, at high phase angles, with quantization and baseline uncertainties. Experience has shown that errors in pointing reconstruction, for observations involving scans, have both random and systematic components. Within a related set of scans, point-to-point errors are usually random, but a systematic shift of the set itself is often present; taken over unrelated groups of scans, however, such systematic offsets are distributed relatively randomly.

TABLE IV

CALCULATED DISK SIGNALS AT HIGH PHASE ANGLES, AS DERIVED FROM IRIS
RADIOMETER MEASUREMENTS

Phase angle α (°)	Radiometer signal, I_{obs} (DN)[a]	Projected FOV radius, r (km)	Model ratio, $F(k, \alpha)$[b]	Disk signal, I (DN)
145.6	6 5 ± 1 0	12,600	0.575	2.73 ± 0.42
145 8	7.5 ± 1.0	10,900	0 504	2 72 ± 0 36
146 5	11 5 ± 1 0	7,120	0.331	2 70 ± 0 23
147 1	13.5 ± 1.0	5,710	0.264	2 54 ± 0 19
148.5	18.5 ± 1 0	3,760	0 172	2 33 ± 0 13
153 2	28 0 ± 1 0	1,780	0.0767	1.78 ± 0 064
154 6	29.0 ± 1 0	1,540	0 0656	1.61 ± 0.056

[a] Quoted error represents random quantization and baseline uncertainty.

[b] Calculated for a Minnaert limb darkening model with $k = 0.38$ (see text). A 20% error in k produces a systematic error of 3% in F.

Thus, we average disk brightnesses calculated from several scans at nearly identical phase angles, and consider their scatter as representing totally random errors.

The use of a Minnaert model and the assumption that the limb darkening parameter derived at a given phase angle is constant over the disk are the principal sources of systematic error in our calculations. Based on the ability of this function to provide a good fit to the data of Tomasko *et al.* (1980) for Saturn, we estimate that the systematic error introduced by the model should be less than 10% for the low and intermediate phase angle calculations. At high phase angles the error should be even less, since an uncertainty of 20% in the limb darkening parameter introduces a systematic error of only 3% into the disk calculations. This relative insensitivity to errors in k is due to the use of a model *ratio* in the calculations.

The integral of the phase curve in DN, weighted by twice the sine of the phase angle, gives the bolometric Bond albedo within a calibration factor. To obtain this integral from the sparsely distributed data provided by the IRIS measurements, we first transform the independent variable from α to $\gamma = \cos(\alpha)$. Then, the phase integral can be expressed in terms of

$$J = 2 \int_{-1}^{1} \phi(\gamma) \, d\gamma,$$

where $\phi(\gamma)$ is the phase curve. We then approximate the phase curve by an interpolant through the IRIS data, giving double weight to the datum at 21.4°, (because the pointing is best determined here) and introducing the additional point $\phi(-1) = 0$. The IRIS data fall naturally into five clusters (Fig. 3), so we use a fourth-order polynomial fit to smooth out the noise without losing the structure of the curve. The resulting interpolant is plotted as the solid line in Fig. 3. The weighted integral over the phase curve is then

$$J = 60.99 \pm 1.64 \text{ DN.}$$

The assigned error is obtained as follows. The random errors associated with each IRIS datum are roughly 6%, as listed in Table IV and shown in Fig. 3. Since the data are clustered in five groups, we then estimate the error in the integral by reducing the single-point percentage error by a factor of $1/\sqrt{5}$.

To obtain the Bond albedo, A, from this integral requires a calibration factor to normalize for the level of incident sunlight and to adjust for the filter response of the instrument (Hanel *et al.* 1981):

$A_{\text{Uranus}} = J$

$$\times \ \frac{(AU_{\text{Uranus}})^2 \times \bar{\tau}_{\text{Diff}} \times p_{\text{Diff}} \times \cos \beta_{\text{Diff}}}{DN_{\text{Diff}} \times (AU_{\text{Diff}})^2 \times \bar{\tau}_{\text{Uranus}}}.$$

From Section 2, the 1 AU-target plate signal, $DN_{\text{Diff}} \times (AU_{\text{Diff}})^2$, is 31193 ± 312 DN. The heliocentric range of Uranus at the time of the planetary observations was 19.1224 AU. The spectrally weighted radiometer transmittances, $\bar{\tau}$, account for the spectral response of the radiometer passband and for the spectrum of the target object; in the calculation of τ_{Uranus} we used the spectrum of Neff *et al.* (1985). (This is only required on a relative scale; we ignore a small time-dependent color change, indicated by a 1.6% increase in $b - y$ between 1981 and 1986, as measured by Lockwood (1987).) We find $\bar{\tau}_{\text{Uranus}} = 0.149 \pm 0.003$, and $\bar{\tau}_{\text{Diff}} = 0.156 \pm 0.002$. The spectrally weighted reflectance of the diffusor plate, p_{Diff}, is 0.497 ± 0.018, and the solar illumination angle of the plate during calibration, β_{Diff}, was 30°. Combining the random errors quadratically and adding them to the systematic uncertainties, the bolometric Bond albedo of Uranus was therefore $A_{\text{Uranus}} = 0.322 \pm 0.049$ at the epoch of the Voyager 2 encounter.

As discussed below (Section 4), the time constant for thermal emission from the Uranian atmosphere is comparable to the orbital period. Thus, it is appropriate to consider the annual mean of the absorbed solar flux in determining the energy balance. The strong latitudinal differences in reflectivity (Fig. 2a) imply that the Bond albedo has a seasonal variation. However, this cannot be determined from Voyager data, since the encounter occurred near summer solstice (the subsolar latitude was −82°), when most of the northern hemisphere was in darkness. Ground-based observations spanning more than three decades show a decrease in disk brightness from northern summer to equinox, followed by an increase into southern summer (Lockwood 1978, Lockwood *et al.* 1983, G. W. Lockwood 1987, personal communica-

tion). Although the pre- and postequinoctal measurements were made with different photometric equipment, so that an absolute comparison for the two summer seasons cannot be made, the observed behavior suggests a roughly symmetric distribution of reflectivity on the two hemispheres of the planet. From the more recent data, Lockwood *et al.* (1983) deduced a 14 ± 5% increase in geometric albedo between near equinoctal conditions in 1961–1963, and a configuration in 1981 which was similar to that observed by Voyager in 1986. On the basis of this result, we reduce our derived albedo by 7 ± 3% to provide an estimate of the annual mean bolometric Bond albedo:

$$\bar{A}_{\text{Uranus}} = 0.300 \pm 0.049.$$

4 THERMAL EMISSION

The global mean thermal emission of the planet is defined by the relation

$$\pi F = \frac{1}{A} \int_A \int_0^\infty \pi F_\nu(\theta, \phi) \, d\nu \, dA,$$

where $\pi F_\nu(\theta, \phi)$ is the thermally emitted spectral flux at wavenumber ν through unit area located at latitude θ and longitude ϕ. The flux is integrated over all wavenumbers and over the entire area A of a planetary reference surface. The spectral flux can be obtained from the radiance at the top of the atmosphere $I_\nu(\mu, \theta, \phi)$ by integration over the upward hemisphere, i.e.,

$$\pi F_\nu(\theta, \phi) = 2\pi \int_0^1 I_\nu(\mu, \theta, \phi)\mu \, d\mu,$$

where μ is the cosine of the emission angle.

Because of limitations in spectral and spatial coverage, it is not possible to evaluate the planetary mean total flux directly from the data. Useful measurements were obtained only within the spectral interval 180 to 400 cm^{-1}, and a relatively small fraction of the total surface area was sampled with good spatial resolution. In addition, the radiance was measured at one or at most only a few emission angles at any given location. Thus, modeling strategies

must be adopted and applied to the available data to obtain an estimate of the planetary mean thermal emission.

We first consider the problem of extrapolation to portions of the spectrum outside of the region actually covered by the measurements. Because of the low temperatures encountered on Uranus, contributions to the total emission at wavenumbers above 400 cm^{-1} are negligible. However, almost 75% of the total emission occurs at wavenumbers below 180 cm^{-1}, so accurate modeling of this region is essential. Within the 180 to 400 cm^{-1} region, sufficient variation in the collision-induced hydrogen opacity exists so that the measurements sample atmospheric levels between approximately 100 and 900 mbar at normal viewing. Essentially all of the planetary thermal emission to space originates within this portion of the atmosphere. Thus, the measured region of the spectrum can be used to retrieve a temperature profile within this critical portion of the atmosphere. If the atmospheric opacity is known, the flux can then be calculated at all wavenumbers using

$$\pi F_\nu = 2\pi \int_0^\infty B_\nu \left[T(z)\right] \frac{\partial}{\partial z} \left[E_3(\tau_\nu)\right] dz,$$

where $E_3(x)$ is the exponential integral of third order

$$E_3(x) = \int_1^\infty \frac{e^{-xy}}{y^3} \, dy,$$

B_ν is the Planck function at wavenumber ν, $z = \ln(p_0/p)$, where p is pressure and p_0 is a reference pressure, τ_ν is the normal optical depth from level z to the top of the atmosphere, and $T(z)$ is the temperature profile.

The dominant source of opacity throughout the spectral region of interest is due to collision-induced hydrogen transitions with contributions from both H_2–H_2 and H_2–He interactions. To model this opacity, a He mole fraction of 0.155 ± 0.033 (Hanel et al. 1986, Conrath et al. 1987) was assumed, with absorption coefficients based on the work of Birnbaum and Cohen (1976), Dore

et al. (1983), Bachet et al. (1983), and Bachet (1986). Within the more nearly transparent portion of the spectrum near 200 cm^{-1}, collision-induced CH_4 opacity is also potentially significant. At the present time, the CH_4 abundance at atmospheric levels of interest is not well constrained; this source of error is discussed further below.

We now consider the problem of spatial sampling. If the thermal emission were uniform over the planetary reference surface, then the flux could be obtained directly from a single measurement taken from sufficiently far away that the planetary disk just fills the instrument field of view. From retrievals of temperatures at different latitudes, however, we know that there is a meridional variation in the tropospheric temperatures as shown in Fig. 2b (Hanel et al. 1986, Flasar et al. 1987). Because of the low temperatures encountered on Uranus and the resulting low signal-to-noise ratio, it is not possible to retrieve detailed temperature profiles from individual spectra. However, it is possible to use data from broad spectral bands to obtain mean temperatures over relatively thick atmospheric layers from individual spectra. The temperatures shown in Fig. 2b were obtained in this way and correspond to mean values for a layer between approximately 400 and 900 mbar. The data were acquired from scans which provided pole-to-pole coverage.

While both poles and the equator are at approximately the same temperature, there are regions at midlatitudes in both hemispheres where the temperatures are 1–2°K lower. This nonuniformity must be taken into account in deriving the planetary mean thermal emission. We have done this by considering the emission at selected latitudes on the planet as indicated in Table V. A reference temperature profile was first obtained by inversion of a mean of 597 spectra obtained at near-normal viewing in the vicinity of the south pole, using standard inversion techniques (Conrath and Gautier 1980). At each of the selected lati-

TABLE V

TEMPERATURE PROFILE CORRECTIONS AND TOTAL
FLUXES AT SELECTED LATITUDES ON URANUS

Latitude (deg)	ΔT (°K)	πF (W cm^{-2} × 10^{-5})
−90	0	7 21
−68	0	7 17
−46	−0.2	7.04
−27	−1 7	6.42
− 4	0	7 04
10	0.2	7 13
40	−0 8	6 79
56	−0.1	7 10
63	0	7.16
72	−0 4	7 01
90	−0.4	7.05

tudes a temperature profile was constructed by first obtaining the difference between the 400–900 mbar temperature at that latitude and at the south pole. This difference was then added to the south polar profile at each atmospheric level. This procedure is justified because most of the emission to space originates from an atmospheric layer between the 400 and 900 mbar pressure levels, and the total flux is quite insensitive to the thermal structure outside of this layer. The adjusted profiles were then used with the known spectral opacity to calculate the total flux emitted between 10 and 400 cm^{-1} at each of the selected latitudes; the results are included in Table V. It is assumed that these fluxes represent the zonal mean value at each latitude although the data shown in Fig. 3 sample only small ranges in longitude. The planetary mean flux was then calculated by linear interpolation between selected latitudes. The result is $\pi F = 6.933$ × 10^{-5} W cm^{-2}, corresponding to an effective planetary temperature $T_{eff} = 59.1$°K.

An alternative approach was also employed in which mean spectra were obtained within selected latitude bins, and a temperature profile was retrieved from each. The profiles were then used to calculate the flux from each bin. One problem with this approach is that in many latitude bands there are relatively few spectra and

the effective noise level of the resulting mean is higher than is generally desirable for the retrieval of complete profiles. In addition, in some regions it is necessary to accept a rather large dispersion in emission angle in order to incorporate even a modest number of spectra in the averages. For these reasons, this approach was employed only as a check on the method described above. The bins used are defined in Table VI where the bin populations and the ranges in emission angle cosine, μ, are also given. The effective temperature obtained in this way is 59.0°K, in good agreement with the previous result.

We must now consider the various sources of error in the determination of the mean flux. These include random and systematic errors in the radiance measurements, and the effects of uncertainties in atmospheric opacities.

Both random and systematic uncertainties have been assessed for the IRIS instruments (Hanel et al. 1980, 1981). The effects of random measurement errors are substantially reduced because of the spectral and spatial integration applied to the data. Since the flux is obtained by vertical integration, it is the mean error in the temperature profile over the levels of significant contribution to the integral which are important.

TABLE VI

LATITUDE BINS AND ASSOCIATED PARAMETERS FOR
DATA USED IN EVALUATING THERMAL FLUX FROM
URANUS

Latitude bin	Population	Range of μ
−90°, −80°	145	0.83–1 0
−80°, −60°	32	0.65–1 0
−60°, −40°	37	0.65–1.0
−40°, −20°	33	0 65–1.0
−20°, 0°	19	0 56–0.80
0°, 20°	11	0.45–0 66
20°, 35°	14	0 56–0 83
35°, 50°	43	0 65–1.0
50°, 60°	35	0.65–1.0
60°, 70°	25	0.87–1.0
70°, 80°	40	0 95–1 0
80°, 90°	137	0 95–1 0

From a knowledge of the noise equivalent spectral radiance of the individual measurements, we estimate that the random error in the retrieved mean temperature in the 400- to 900-mbar layer is approximately 0.1°K. This results in an error in the calculated flux of $\pm 0.033 \times 10^{-5}$ W cm^{-2}. Errors in the assumed atmospheric opacities enter both in the retrieval of the south polar temperature profile and in the subsequent calculation of the total flux (see, e.g., Gautier *et al.* 1981). As mentioned above, the CH$_4$ abundance is not well constrained in the atmospheric layers which are significant for our purpose. The above results were obtained without CH$_4$ opacity included in either the south pole temperature retrieval or the subsequent flux calculations. If significant CH$_4$ opacity is present, the errors introduced into the temperature profile tend to cancel when the flux is calculated, provided that the CH$_4$ opacity is uniform in latitude. If the CH$_4$ abundance is nonuniform, then significant uncertainties can be introduced. To estimate the possible magnitude of this error, we consider a situation in which the south polar region is CH$_4$-free, while for the remainder of the planet the CH$_4$ is at its saturation value; the CH$_4$ absorption coefficients employed are based on a model provided by G. Orton (1986, personal communication). In this case, we obtain an error of $\pm 0.070 \times 10^{-5}$ W cm^{-2} in the flux.

Another source of error in the atmospheric opacity is the uncertainty in the determination of the He mole fraction, currently estimated to be 0.155 ± 0.033 (Conrath *et al.* 1987). Again, this will introduce an uncertainty in the retrieved profile as well as in the flux calculations. In this case there is less tendency for cancellation of errors since the extrapolated portion of the spectrum (at wavenumbers below 180 cm^{-1}) is more sensitive to the helium abundance than is the measured portion above 180 cm^{-1}, where the temperature profile is retrieved. This results in a flux error of $\pm 0.10 \times 10^{-5}$ W cm^{-2}.

We have not included opacity due to

TABLE VII

SUMMARY OF ERRORS FOR THERMAL EMISSION DETERMINATION

Source	Magnitude (W cm^{-2})	% Error
Random noise	3.26×10^{-7}	0 5
He abundance	$10\ 0\ \times 10^{-7}$	1 4
CH$_4$ abundance	$7\ 0\ \times 10^{-7}$	1.0
RMS	$12\ 6\ \times 10^{-7}$	1.9

clouds and hazes in our calculations; if such material is present, it could introduce another source of error. Hanel *et al.* (1986) have argued against the likelihood that cloud opacity significantly affects the infrared spectrum within the regions of interest here; therefore, we conclude that uncertainties in cloud opacities contribute little to the flux error.

If we quadratically combine the estimated errors listed in Table VII, we finally obtain

$$\pi F = (6.93 \pm 0.13) \times 10^{-5} \text{ W cm}^{-2}$$

which corresponds to an effective temperature

$$T_{\text{eff}} = 59.1 \pm 0.3°K.$$

The atmospheric radiative time constant exceeds the planetary orbital period. Hence, the temperature at the radiation-to-space level varies with a small annual amplitude and a phase lag of a full season (Bezard and Gautier 1985, Conrath *et al.* 1989). On this basis, our value for the effective temperature (derived near solstice) is expected to differ from the annual mean by less than 0.1°K.

5. DISCUSSION

Full-disk observations of Uranus have been made by the Voyager 1 Imaging experiment over a range of phase angles. Data for clear and orange filters are presented as normalized phase curves by Pollack *et al.* (1986); each curve is normalized to unity at a different phase angle (43° for clear, and
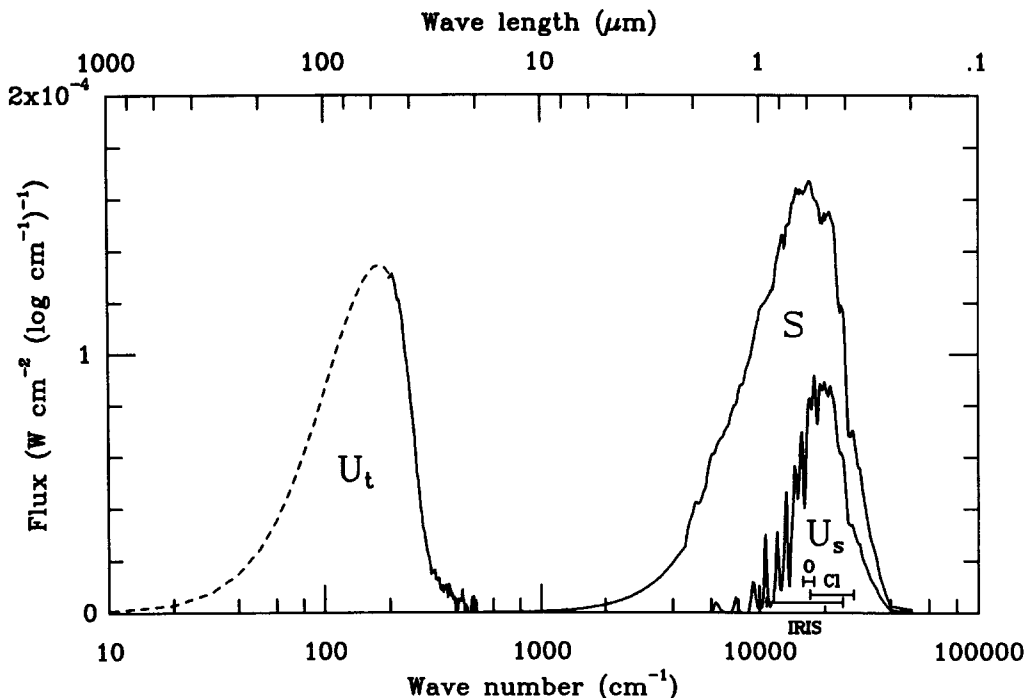
FIG. 4 Global mean fluxes appropriate to the Uranian heat balance Curve U_t represents the thermal spectrum of Uranus; the solid portion is from IRIS data at 4.3 cm⁻¹ resolution, while the dashed part is an extrapolation calculated from the known atmospheric composition and temperature profile, using a radiative transfer program Curve S is the solar spectrum, reduced to a spectral resolution of 50 cm⁻¹ Curve U_s is the reflected solar spectrum of Uranus (at 10 cm⁻¹ resolution) for a bolometric Bond albedo of 0.300. Horizontal bars represent the spectral ranges which contain the central 90% of the energy collected by the orange (O) and clear (Cl) filters of the narrow angle Voyager camera, and by the IRIS radiometer (IRIS).

49° for orange). However, when the data for the two filters are normalized at a single-phase angle, then the remaining data agree among the filters for all other angles, i.e., the phase curves in the two colors are identical within an unspecified scale factor. For comparison with present results, we have renormalized these data by scaling them to match the IRIS-derived disk brightness at 54° (first linearly interpolating between the points derived from images at 49° and 58° to a phase angle of 54°). The resulting values are plotted in Fig. 3, together with the 10% uncertainties quoted by Pollack *et al.* The spectral bandpasses of the imaging filters differ from that of the IRIS radiometer (Fig. 4), but the three sets of results are quite consistent.

By directly obtaining the absolute phase curve of Uranus, we have evaluated the Bond albedo without making separate determinations of the geometric albedo and the phase integral. However, estimates of these quantities can now be made from the phase curve. The zero-phase intercept in Fig. 3 (43.70 DN) yields a geometric albedo $p_{Uranus} = 0.231$ at the time of the Voyager 2 encounter. Since the intercept represents a model extrapolation, it is subject to greater uncertainty than is the fit at intermediate phase angles. We, therefore, increase the assigned random error to 10%. Including the systematic uncertainty in the error yields $p_{Uranus} = 0.231 \pm 0.048$ at the time of the encounter. Making the seasonal adjustment gives the annual mean:

$$\bar{p}_{\text{Uranus}} = 0.215 \pm 0.046.$$

Combining the geometric and Bond albedos provides an estimate for the phase integral:

$$\bar{q}_{\text{Uranus}} = \frac{\bar{A}_{\text{Uranus}}}{\bar{p}_{\text{Uranus}}} = 1.40 \pm 0.14.$$

The uncertainty is less than that implied by the total quoted uncertainties in $\bar{A}$ and $\bar{p}$ due to cancellation of the systematic errors associated with the Minnaert modeling.

The present results are based entirely on IRIS measurements obtained during the Voyager flyby. Pollack et al. (1986) have combined spacecraft and ground-based observations through detailed physical models of the Uranian atmosphere to obtain the bolometric Bond albedo and phase integral. Their results are tied to the determination of the spectral geometric albedo by Neff et al. (1985). An independent determination of the spectral geometric albedo has been made by Lockwood et al. (1983). Data for all of these investigations were obtained during the period 1981–1986, when there was little change in the aspect Uranus presented to the Sun. The results, adjusted for the Voyager-determined planetary figure, are compared in Table VIII.

Our principal result on the reflective properties of Uranus, the bolometric Bond albedo, lies within one-half standard error of the value derived by Pollack et al. The geometric albedo and phase integral differ by approximately one standard error from the other derived values; it is likely that the

discrepancies are due to the behavior of the phase curve below 15° phase angle (Fig. 3).

Over the 3° range of phase angles accessible from Earth, observed values of the mean phase coefficient are 0.0014 ± 0.0004 and 0.0029 ± 0.0011 mag deg^{-1} in b and y filters, respectively (Lockwood 1977), and 0.0017 ± 0.0002 mag deg^{-1} in the B filter (Lockwood 1978). We note that, by fitting the IRIS phase curve data with a polynomial in $\gamma = \cos(\alpha)$, the resulting interpolant has a zero phase coefficient; over the first 3°, its mean phase coefficient is 0.0008 mag deg^{-1}, which is less than half the average of the above values. If the actual phase curve lies above our extrapolation at phase angles below 15°, then it can be expected to have sharper curvature near zero phase. This will increase the phase coefficient and the albedos (affecting the geometric albedo more than the Bond albedo). The tendency will therefore be to improve the agreement among all determined quantities; thus, raising the extrapolated portion of the phase curve to increase the geometric albedo by 10–15% (well within our derived uncertainties) would bring all of the IRIS-derived quantities to within one-half standard error of all other determinations.

To evaluate the energy balance requires specification of the planetary figure. At the 1-bar level, Lindal et al. (1987) have determined that $R_{\text{eq}} = 25559 \pm 4$ km, and $R_{\text{pole}} = 24973 \pm 20$ km, giving an oblateness $\varepsilon = 0.0229 \pm 0.0008$. We take the radiating level for thermal emission as the level where the

TABLE VIII

DETERMINATIONS OF BOLOMETRIC ALBEDOS AND PHASE FUNCTIONS OF URANUS FOR EPOCH 1981–1986

Reference	p	q	A
Lockwood et al (1983)	0 264 $\pm$ 0 008[a]	—	—
Neff et al (1985)	0 27 $\pm$ 0 02[a]	—	—
Pollack et al. (1986)	—	1.26 $\pm$ 0.11[b]	0.343 $\pm$ 0.055[l]
This investigation	0.231 $\pm$ 0.048	1 40 $\pm$ 0.14	0.322 $\pm$ 0.049

[a] Ground-based observations, adjusted to the 25,582-km equatorial radius used in the present investigation.

[b] Derived using models fitted to Voyager imaging data and the spectral geometric albedos of Neff et al. (1985)

TABLE IX

THE ENERGY BALANCE OF THE OUTER PLANETS

Parameter	Jupiter[a]	Saturn[b]	Uranus[c]	Neptune
Geometric albedo	0.274 ± 0 013	0 242 ± 0.012	0.215 ± 0 046	0.25 ± 0 02[d]
Phase integral	1 25 ± 0.1	1 42 ± 0 1	1 40 ± 0 14	1 25 ± 0.10[e]
Bond albedo	0.343 ± 0 032	0 342 ± 0 030	0 300 ± 0.049	0 31 ± 0.04
Absorbed power (10^{16} W)	50 14 ± 2 48	11.14 ± 0 50	0 526 ± 0 037	0 20 ± 0 01
Equilibrium temperature (°K)	109 5 ± 1 4	82 4 ± 0 9	58 2 ± 1 0	46 2 ± 0 6
Emitted power (10^{16} W)	83 65 ± 0 84	19 77 ± 0 32	0 560 ± 0.011	0 52 ± 0.07
Effective temperature (°K)	124.4 ± 0 3	95 0 ± 0 4	59 1 ± 0 3	59 1 ± 2.0[f]
Energy balance	1 67 ± 0 09	1 78 ± 0 09	1 06 ± 0 08	2 7 ± 0.4
Internal power (10^{16} W)	33 5 ± 2 6	8 63 ± 0 60	0.034 ± 0 038	0 33 ± 0 07
Internal energy flux (10^{-4} W/cm²)	5 44 ± 0.43	2 01 ± 0 14	0.042 ± 0 047	0 43 ± 0 09
Internal power/unit mass (10^{-11} W/kg)	17 6 ± 1.4	15.2 ± 1 1	0.392 ± 0 441	3 2 ± 0 7
Luminosity: $\log(L/L_\odot)$	−9 062 ± 0.034	−9 651 ± 0 030	$-12.054^{+0\ 327}_{-}$	−11 08 ± 0 10

[a] Hanel *et al* (1981)
[b] Hanel *et al* (1983).
[c] This investigation
[d] Neff *et al*. (1985).
[e] Pollack *et al* (1986)
[f] Orton (1985).

tropospheric temperature equals the effective temperature. This occurs at approximately 430 mbar, or 23 km higher than the 1-bar surface. Because of the long absorption path length at the limb, the effective altitude for absorption of solar radiation is expected to occur somewhat higher. However, since we have no satisfactory way of determining this increase, we use the dimensions of the planet at the radiating level to calculate the annual mean cross section. This is a conservative assumption, in the sense that a larger effective radius will systematically reduce the calculated energy balance (an increase of 125 km would reduce the energy balance by 1%).

We evaluate the equilibrium temperature implied by the mean bolometric Bond albedo (Section 3), using a solar constant $S = 0.1374 \pm 0.0007$ W cm^{-2} (Willson *et al*. 1980), mean solar distance for Uranus $R = 19.28$ AU, and the seasonally averaged cross section for solar radiation to obtain $T_{eq} = 58.2 \pm 1.0$°K. Thus, the energy balance, E, is

$$E = \left(\frac{T_{eff}}{T_{eq}}\right)^4 = 1.06 \pm 0.08$$

(if the mean Bond albedo from Pollack *et al*. is used, $E = 1.09 \pm 0.09$). Our results are summarized in Table IX. The 1σ upper limit of 1.14 is substantially lower than the energy balance of Jupiter or Saturn. It is also lower than previous upper limit estimates for Uranus (see Table I). The value is consistent with an absence of helium separation, for which there is independent evidence in the nearly solar helium abundance within the outer layers of the planet (Conrath *et al*. 1987).

Because of the extreme obliquity of Uranus, the annually averaged solar input to the poles exceeds that at the equator. Thus, a mechanism is required for the advection of absorbed solar energy in order to explain the nearly uniform latitudinal distribution of atmospheric temperatures (Fig. 2b). Friedson and Ingersoll (1987) have shown that, for values of the energy balance as low as we have derived, a significant part of the required meridional transport takes place in a fairly shallow layer of the atmosphere, rather than through deep convection.

Various interior models of Uranus suggest a large mass ratio of "ice" to "rock,"

with as little as one to three Earth masses of "rock," e.g., Podolak and Reynolds (1987). Based on the estimated terrestrial heat flux of $(4.3 \pm 0.6) \times 10^{13}$ W (Williams and von Herzen 1974), radiogenic heating from a similarly composed core can only account for 15–50% of the formal excess we have determined for Uranus.

Stevenson (1987) has proposed a novel means of suppressing deep convection, and thereby limiting the internal energy flux. In models that fit the known planetary constraints (mass, H_2–He ratio, energy balance, rotation period, oblateness, and gravitational moments), significant compositional gradients are postulated which prevent convection, even in the presence of superadiabatic lapse rates. In distinction to the results of Podolak and Reynolds (1987), these models suggest that the ice : rock ratio is of order unity, thereby allowing perhaps 5–6 Earth masses of rock in Uranus; in this case, the observed 1σ energy flux could be largely accounted for by radiogenic heat.

The full implications of the small internal energy source of Uranus remain to be established. Additional insights may be obtained as results of the detailed study of Neptune which will become possible following the Voyager 2 flyby on August 25, 1989.

REFERENCES

BACHET, G. 1986. Collision induced spectra of the H_2–He interaction from 79 K to 248 K between 200 and 700 cm^{-1}. *Bull. Amer Astron Soc* **18**, 719

BACHET, G., E R COHEN, P DORE, AND G BIRNBAUM 1983 The translational–rotational absorption spectrum of hydrogen. *Canad. J. Phys.* **61**, 591

BEZARD, B , AND D GAUTIER 1985 A model of the spatial and temporal variations of the Uranus thermal structure In *The Jovian Atmospheres* (M Allison and L Travis, Eds), NASA Conference Publication 2441, Vol 254

BIRNBAUM, G., AND E. R. COHEN 1976. Theory of the line shape in passive induced absorption. *Canad. J. Phys.* **54**, 593.

CONRATH, B. J., AND D. GAUTIER 1980 Thermal structure of Jupiter's atmosphere obtained by inversion of Voyager 1 infrared measurements In *Remote Sensing of Atmospheres and Oceans* (A Deepak, Ed.) Academic Press, New York

CONRATH, B. J., D GAUTIER, R A. HANEL, AND J. S. HORNSTEIN 1984 The helium abundance of Saturn from Voyager measurements *Astrophys. J* **282**, 807.

CONRATH, B. J., D. GAUTIER, R A. HANEL, G. LINDAL, AND A. MARTEN 1987. The helium abundance of Uranus from Voyager measurements *J. Geophys Res* **92**, 15003.

CONRATH, B. J., P J GIERASCH, AND S. S LEROY 1989. Temperature and circulation in the stratospheres of the outer planets *Icarus*, in press

COURTIN, R , P LENA, M DeMUIZON, D ROUAN, C. NICOLLIER, AND J. WIJNBERGEN 1979. Far infrared photometry of planets: Saturn and Venus. *Icarus* **38**, 411

DORE, P., L. NENCINI, AND G. BIRNBAUM 1983 Far infrared absorption in normal H_2 from 77 K to 298 K. *J. Quant Spectrosc. Radiat. Transfer* **30**, 245

FLASAR, F M , B. J CONRATH, P. J. GIERASCH, AND J A. PIRRAGLIA 1987. Voyager infrared observations of Uranus' atmosphere. Thermal structure and dynamics. *J. Geophys. Res.* **92**, 15011

FRIEDSON, J., AND A. P. INGERSOLL 1987. Seasonal meridional energy balance and thermal structure of Uranus. A radiative–convective–dynamical model. *Icarus* **69**, 135

GAUTIER, D., B. J. CONRATH, F. M. FLASAR, R. A HANEL, V G. KUNDE, A CHEDIN, AND N. SCOTT 1981 The helium abundance of Jupiter from Voyager. *J Geophys Res* **86**, 8713.

GRABOSKE, H J , JR , R J. OLNESS, AND A. S GROSSMAN 1975. Thermodynamics of dense hydrogen–helium fluids. *Astrophys. J.* **199**, 255.

HANEL, R. A., B. J. CONRATH, F. M FLASAR, V G KUNDE, W C MAGUIRE, J. C. PEARL, J A PIRRAGLIA, R SAMUELSON, D. CRUIKSHANK, D. GAUTIER, P GIERASCH, L. HORN, AND P SCHULTE 1986. Infrared observations of the Uranian system *Science* **233**, 70.

HANEL, R. A., B J CONRATH, L W HERATH, V. G. KUNDE, AND J A PIRRAGLIA 1981 Albedo, internal heat and energy balance of Jupiter. Preliminary results of the Voyager infrared investigation. *J Geophys. Res* **86**, 8705

HANEL, R. A , B. J CONRATH, V G. KUNDE, J. C PEARL, AND J A PIRRAGLIA 1983. Albedo, internal heat flux, and energy balance of Saturn. *Icarus* **53**, 262.

HANEL, R A., D CROSBY, L. HERATH, D VANOUS, D. COLLINS, H CRESWICK, C HARRIS, AND M RHODES 1980 Infrared spectrometer for Voyager *Appl. Opt* **19**, 1391

HILDEBRAND, R. H , R. F. LOEWENSTEIN, D. A. HARPER, G S ORTON, J KEEN, AND S. E WITHCOMB 1985. Far-infrared and submillimeter brightness temperatures of the giant planets. *Icarus* **64,** 64.

HUBBARD, W B., AND R. SMOLUCHOWSKI 1973 Structure of Jupiter and Saturn *Space Sci Rev* **14,** 599

LINDAL, G. F., J. R. LYONS, D. N. SWEETNAM, V R ESHLEMAN, D. P. HINSON, AND G. L. TYLER 1987. The atmosphere of Uranus. Results of radio occultation measurements with Voyager 2. *J Geophys Res.* **92,** 14987

LOCKWOOD, G. W. 1977. Secular brightness increases of Titan, Uranus, and Neptune, 1972–1976 *Icarus* **32,** 413.

LOCKWOOD, G W 1978 Analysis of photometric variations of Uranus and Neptune since 1953 *Icarus* **35,** 79.

LOCKWOOD, G. W., B L LUTZ, D. T THOMPSON, AND A. WARNOCK III 1983 The albedo of Uranus *Astrophys. J.* **266,** 402

NEFF, J S., D C HUMM, J T BERGSTRALH, A L COCHRAN, W D COCHRAN, E S BARKER, AND R G. TULL 1984 Absolute spectrophotometry of Titan, Uranus, and Neptune· 3500–10,500 Å *Icarus* **60,** 221.

NEFF, J. S , T. A. ELLIS, J. APT, AND J T BERGSTRALH 1985. Bolometric albedos of Titan, Uranus, and Neptune. *Icarus* **62,** 425

ORTON, G S. 1985. A pre-Voyager infrared perspective of the atmosphere of Uranus *Bull. Amer Astron. Soc.* **17,** 745.

PODOLAK, M., AND R. T. REYNOLDS 1987. The rotation rate of Uranus, its internal structure, and the process of planetary accretion *Icarus* **70,** 31.

POLLACK, J B , A S. GROSSMAN, R MOORE, AND H C GRABOSKE, JR 1977 A calculation of Saturn's gravitational contraction history. *Icarus* **30,** 111

POLLACK, J B., K RAGES, K. H. BAINES, J T BERGSTRALH, D. WENKERT, AND E DANIELSON 1986.

Estimates of the bolometric albedos and radiation balance of Uranus and Neptune. *Icarus* **65,** 442

SALPETER, E. 1973. On convection and gravitational layering in Jupiter and stars of low mass. *Astrophys J.* **181,** L83

SMITH, B A , L. A SODERBLOM, R. BEEBE, D BLISS, J M BOYCE, A. BRAHIC, G A BRIGGS, R. H. BROWN, S. A COLLINS, A. F COOK II, S K CROFT, J N. CUZZI, G E. DANIELSON, M E. DAVIES, T E DOWLING, D GODFREY, C J. HANSEN, C HARRIS, G E HUNT, A P INGERSOLL, T V JOHNSON, R. J KRAUSS, H MASURSKY, D MORRISON, T OWEN, J B PLESCIA, J B POLLACK, C. C PORCO, K RAGES, C SAGAN, E M. SHOEMAKER, L A SROMOVSKY, C STOKER, R G STROM, V E SUOMI, S P SYNNOTT, R J TERRILE, P THOMAS, W R THOMPSON, AND J VEVERKA 1986 Voyager 2 in the Uranian system. Imaging science results *Science* **233,** 43

SMOLUCHOWSKI, R 1967. Internal structure and energy emission of Jupiter *Nature (London)* **215,** 691.

STEVENSON, D. J. 1987. Uranus *Bull. Amer. Astron Soc.* **19,** 851

STEVENSON, D J , AND E. E SALPETER 1976 Interior models of Jupiter. In *Jupiter* (T Gehrels, Ed) Univ of Arizona Press, Tucson.

TOMASKO, M G , R. S MCMILLAN, L R DOOSE, N D CASTILLO, AND J. P DILLEY 1980. Photometry of Saturn at large phase angles. *J. Geophys Res* **85,** 5891

TOMASKO, M G , R. A. WEST, AND N D. CASTILLO 1978 Photometry and polarimetry of Jupiter at large phase angles I Analysis of imaging data of a prominent belt and a zone from Pioneer 10. *Icarus* **33,** 558

WILLIAMS, D. L., AND R P VON HERZEN 1974 Heat loss from the Earth. New estimate *Geology* **2,** 327

WILLSON, R. C., C. H. DUNCAN, AND J. GEIST 1980. Direct measurements of solar luminosity variation. *Science* **207,** 177